Author(s): Geng, Zhuoran; Maasilta, Ilari J.

Title: Complete tunneling of acoustic waves between piezoelectric crystals

Year: 2023

Version: Published version
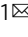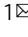
ARTICLE

Complete tunneling of acoustic waves between piezoelectric crystals

Zhuoran Geng [1 ✉] & Ilari J. Maasilta [1 ✉]

The mechanical displacements in piezoelectric materials carry along macroscopic electric fields, allowing tunneling of acoustic waves across a vacuum gap beyond the charge-charge interaction distance. However, no rigorous proof of complete acoustic wave tunneling has been presented, and the conditions to achieve complete tunneling have not been identified. Here, we demonstrate analytically the condition for such phenomenon for arbitrary anisotropic crystal symmetries and orientations, and that complete transmission of the incoming wave occurs at the excitation frequency of leaky surface waves. We also show that the complete transmission condition can be related to the surface electric impedance and the effective surface permittivity of the piezoelectric material, relevant to realize the complete tunneling experimentally. We support our findings with numerical results for the maximum power transmittance of a slow transverse wave tunneling between identical ZnO crystals. The results show that complete tunneling can be achieved for a large range of orientations.

[1] Nanoscience Center, Department of Physics, University of Jyvaskyla, P. O. Box 35, FI-40014 Jyväskylä, Finland. ✉email: zhgeng@jyu.fi; maasilta@jyu.fi

A coustic waves (acoustic phonons) are deformations or vibrations propagating through a material medium. As such, they do not exist in vacuum, leading to the initial conclusion that it is impossible for the vacuum to transmit the energy of an acoustic wave between two separated media. However, at the atomic scale the vibrations of the nuclei can propagate via their electrical interactions through vacuum. Thus, a question can be raised, whether acoustic phonons can also be transmitted across larger than atomic scale vacuum gaps through some electromagnetic mechanism. This is a relevant question, as with the advances in experimental techniques, nanometer to sub-nanometer scale vacuum gaps can be achieved[1–4]. The possibility of such acoustic phonon tunneling, as it is often called in the literature, has attracted a considerable amount of theoretical work in recent years to investigate possible mechanisms of the effect such as Casimir and van der Waals forces, particularly in the context of near-field heat transfer[5–18].

One possible mechanism for acoustic wave tunneling is piezoelectricity, as in piezoelectric materials mechanical displacements carry along macroscopic electric fields. When an acoustic wave in a piezoelectric solid impinges on a free surface, it extends a decaying, evanescent electric field into the vacuum[19]. The length scale of this decay is determined by the wavelength of the acoustic wave, so by bringing another piezoelectric solid within a wavelength, acoustic power can be transmitted into the second piezoelectric solid across the vacuum gap. What makes this piezoelectrically mediated acoustic wave tunneling particularly attractive is its length scale: it is not fixed to be in the nanoscale, but operates on the typically much larger wavelength scale defined by the frequency (1 GHz would correspond to ~5 μm). The effect was introduced[20,21] and observed[22] long ago (for more detailed background, see Geng and Maasilta[23]), but developed further more recently[5,23,24]. In particular, a general formalism was introduced[23] that is applicable to any incident bulk wave mode for any anisotropic crystallographic orientation. One of the most interesting suggestions[5,21,24] is the possibility of unity transmission for some particular conditions, meaning that the incident wave could perhaps be completely transmitted into the adjacent solid. However, the discussions in previous literature[5,21,24] are limited either by the simplified models used, or only show numerical results for the highest symmetry crystal orientations. Until now, no rigorous proof of complete acoustic wave tunneling has been presented, nor have generally valid complete tunneling conditions been put forward.

In this work, we focus on the power transmittance of acoustic wave tunneling. We use the general formalism developed for piezoelectric acoustic wave tunneling[23] to analytically prove the existence of the complete tunneling phenomenon between two vacuum separated identical solids. In addition, a resonant tunneling condition is also derived, corresponding to the excitation of leaky surface waves. We also propose that this condition could be checked experimentally. Further discussion of the results are presented with a few numerical examples for ZnO crystals. In particular, we find our results differ from those obtained before[5].

Results and discussion

Tunneling of acoustic waves. We study a system of two aniso-tropic, semi-infinite piezoelectric solids separated by a vacuum gap of width d, as shown in Fig. 1. Two coordinate systems describe the relation between the crystal intrinsic orientation, denoted by XYZ, and the external laboratory space, denoted by xyz. The surfaces of the solids are assumed to be mechanically and electrically free[23], with surface normals aligned with the z-axis. We consider an incoming homogeneous acoustic plane (bulk) wave $\sim \exp(-i\mathbf{k} \cdot \mathbf{r} + i\omega t)$, where $\mathbf{k}$ and ω are the wave
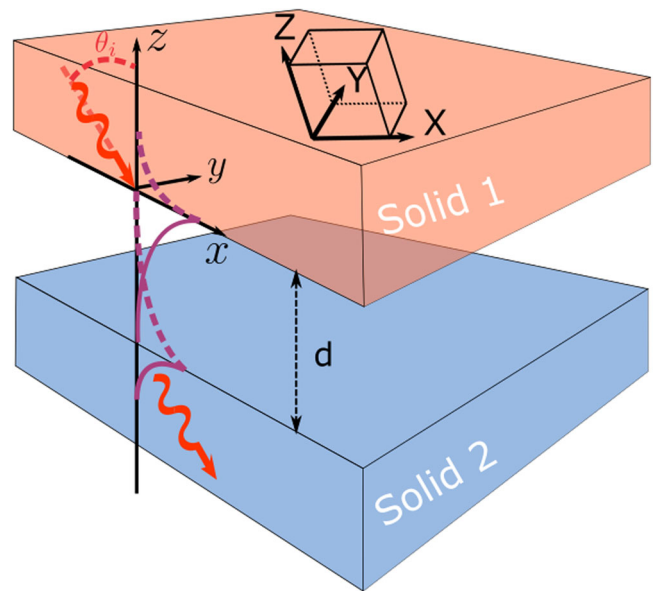

Fig. 1 Schematic of the system under study. Two piezoelectric solids 1, 2 are separated by a vacuum gap of width d. An incoming acoustic wave from solid 1 (positive z-axis of a laboratory coordinates xyz) with an incident angle θ_i tunnels across the vacuum gap into solid 2 inside the xz-plane. XYZ describe the intrinsic crystal coordinates, which can be rotated w.r.t. the xyz coordinates.

vector and angular frequency, propagating inside the xz-plane (sagittal plane) from the positive z-axis direction toward the surface at $z = 0$, with a positive x-component of wave vector ($k_x > 0$). In addition, we only consider low frequency acoustic waves with linear dispersion and assume the usual quasistatic approximation for piezoelectric acoustic waves[19] satisfying $\mathbf{E} = -\nabla \Phi$, where $\mathbf{E}$ and Φ are the electric field and the electric potential, respectively.

An incident bulk wave scatters into a linear combination of partial waves at an interface. These partial waves are either reflected or transmitted, and can either be homogeneous (bulk) waves or inhomogeneous (evanescent) waves bound on the surface of the solid[23]. The single surface reflection and transmission coefficients, which describe the amplitudes of these scattered waves, can be calculated following the multiple reflection method presented in Section III.B in Geng and Maasilta[23]. We denote these coefficients with an overhead bar, as follows: $\bar{t}^{(1)}_{\text{in} \to \text{V}}$ is the coefficient of an incoming wave from solid 1 transmitted into a vacuum electric wave, $\bar{t}^{(2)}_{\text{V} \to \alpha}$ is the coefficient of an vacuum wave transmitted into mode α in solid 2, and $\bar{r}^{(i)}_{\text{V}}$ is the coefficient of an vacuum wave reflected on the vacuum side of the interface of solid $i = 1, 2$. In these coefficients, $\alpha = 1, ..., 4$ correspond to the four physically allowed electroacoustic partial wave modes in the corresponding solids 1 or 2. It should be noted that these coefficients are not the direct analogs of the Fresnel coefficients[25] from optics.

A total transmission coefficient t_α, which describes the amplitude ratio of a transmitted partial wave α in solid 2 to an incoming bulk wave from solid 1, takes a form[23] (for details, see "Methods" section):

$$t_\alpha = \frac{\bar{t}^{(1)}_{\text{in} \to \text{V}} \bar{t}^{(2)}_{\text{V} \to \alpha}}{e^{k_x d} - \bar{r}^{(1)}_{\text{V}} \bar{r}^{(2)}_{\text{V}} e^{-k_x d}} = \bar{t}^{(1)}_{\text{in} \to \text{V}} \bar{t}^{(2)}_{\text{V} \to \alpha} f_m(d), \quad (1)$$

with k_x the wave vector component along the surfaces, which is conserved in the tunneling process. This expression can be interpreted as two single surface transmission

coefficients $\bar{t}_{\text{in}\to\text{V}}^{(1)}$ and $\bar{t}_{\text{V}\to\alpha}^{(2)}$ coupled by a geometrical multiple reflection factor for evanescent electrical waves in the gap $f_\text{m}(d) = [\exp(k_x d) - \bar{r}_\text{V}^{(1)}\bar{r}_\text{V}^{(2)}\exp(-k_x d)]^{-1}$ [23]. It implicitly depends on the incident angle θ_i not only via $k_x = k\sin\theta_i$, but also via the coefficients $\bar{t}$ and $\bar{r}$, which are functions of $v_x = \omega/(k\sin\theta_i)$ ("Methods").

Derivation of the condition for complete tunneling. To fully describe the tunneling of the acoustic wave, we also look at the energy transfer between the solids. The time-averaged power flow density (energy flux, units [Wm^{-2}]) of a transmitted partial wave in the direction normal to the surfaces (denoted as P_α) can be obtained from the real part of the normal component of piezo-electric Poynting vector ("Methods"). For the tunneled bulk partial waves, the transmitted power relates to the normal component of the incident power by $P_\alpha = |t_\alpha|^2 P_\text{in}$, in which the input power P_in can be from a coherent bulk wave or from a thermal phonon, whereas the reflected or transmitted evanescent partial waves in solids 1,2 are bound onto the surface and carry no power in the normal direction ($P_\alpha = 0$ if α is an evanescent mode).

As there is no dissipation inside the vacuum gap, the normal direction power flow density inside the vacuum (denoted by P_V) is equal to the total normal direction transmitted power density (denoted by P_Σ). It is clear that P_Σ is the sum of P_α over all the transmitted *bulk* waves in solid 2, and we can write it using Eq. (1) as $P_\Sigma = \sum_\alpha |\bar{t}_{\text{in}\to\text{V}}^{(1)}\bar{t}_{\text{V}\to\alpha}^{(2)} f_\text{m}(d)|^2 P_\text{in}$, where α runs only over the bulk modes. The number of transmitted bulk modes can be from zero to three (in some cases four[26]), and if there is no bulk mode available, the power flow in both the vacuum and solid 2 are zero. On the other hand, the normal power flow inside the vacuum gap can be expressed using the Poynting's theorem under the quasistatic approximation as $P_\text{V} = 2|\bar{t}_{\text{in}\to\text{V}}^{(1)} f_\text{m}(d)|^2 \text{Re}[\bar{r}_\text{V}^{(2)}] P_\text{in}$ (see Supplementary Note 1 for the derivation). As a result, from $P_\text{V} = P_\Sigma$ we find a relation:

$$2\text{Re}\left[\bar{r}_\text{V}^{(2)}\right] = \sum_{\alpha=\text{bulk}} |\bar{t}_{\text{V}\to\alpha}^{(2)}|^2. \qquad (2)$$

Furthermore, if we assume that the two solids consist of the same material with identical crystal orientations, two additional relations that link the single surface coefficients of the two solids can be found by exploiting the completeness of the eigensolutions of the scattering problem (see Supplementary Note 2 for the derivations). The first one relates the reflection coefficients $\bar{r}_\text{V}^{(i)}$ of the two solids as:

$$\bar{r}_\text{V} \equiv \bar{r}_\text{V}^{(2)} = -\bar{r}_\text{V}^{(1)}. \qquad (3)$$

The second one states that if the transmitted bulk wave mode γ in the solid 2 is the same mode as the incident wave in solid 1, there exists a relation:

$$\bar{t}_{\gamma\to\text{V}}^{(1)} = \bar{t}_{\text{V}\to\gamma}^{(2)}. \qquad (4)$$

In addition, by comparing the relation (4) with Eq. (2), we find the condition:

$$2\text{Re}(\bar{r}_\text{V}) \geq |\bar{t}_{\text{in}\to\text{V}}^{(1)}|^2, \qquad (5)$$

where the equality is satisfied when there exists only one transmitted bulk wave mode in solid 2 and the mode is the same as the incident wave in solid 1. By applying the relations (2) and (3), P_Σ can then be simplified to:

$$\frac{P_\Sigma}{P_\text{in}} = \frac{2\text{Re}(\bar{r}_\text{V})|\bar{t}_{\text{in}\to\text{V}}^{(1)}|^2}{4\text{Re}(\bar{r}_\text{V})^2 + \left(e^{2k_x d} - |\bar{r}_\text{V}|^2\right)^2 e^{-2k_x d}}, \qquad (6)$$

which explicitly depends only on two single surface coefficients: $\bar{t}_{\text{in}\to\text{V}}^{(1)}$ and $\bar{r}_\text{V}$.

Equation (6) shows that the total transmitted power P_Σ is always less than the incident power P_in if more than one transmitted bulk wave modes exist, since in that case the inequality Eq. (5) takes the greater-than sign. This result has the implication that complete tunneling, i.e., the full transmission of the incident power, can't be achieved if the transmitted wave consists of multiple partial bulk waves, in contradiction to previous work[5].

In contrast, if there is only one transmitted homogeneous bulk mode and it is the same mode as the incident wave, then the equal sign of Eq. (5) is valid, and Eq. (6) simplifies to:

$$\frac{P_\Sigma}{P_\text{in}} = \frac{4\text{Re}(\bar{r}_\text{V})^2}{4\text{Re}(\bar{r}_\text{V})^2 + \left(e^{2k_x d} - |\bar{r}_\text{V}|^2\right)^2 e^{-2k_x d}}, \qquad (7)$$

which very much resembles the Fabry-Perot-like form of transmission coefficients for the near-field radiative heat transfer[27]. From Eq. (7), it is clear that the maximum transmitted power is exactly equal to the incident power ($P_\Sigma = P_\text{in}$) when the resonance condition:

$$|\bar{r}_\text{V}| = e^{k_x d}, \qquad (8)$$

is satisfied, similar to the corresponding condition for perfect photon tunneling in near-field heat transfer[28,29]. This proves that (1) unity transmission (complete tunneling) of an acoustic wave across a vacuum gap is possible, and (2) the condition for it depends explicitly only on the single surface reflection coefficient $\bar{r}_\text{V}$, the wave vector component k_x and the gap width d. The physical explanation of such complete tunneling is the excitation of resonant coupled leaky surface waves on both interfaces (more details below and in Supplementary Note 4), which is fundamentally different from the principle of antireflection in optics[25].

In particular, with a given material and crystal orientation, $\bar{r}_\text{V}$ is only a function of the incident angle and is independent of the gap width or the existence of the adjacent solid. We propose that, as a material parameter, $\bar{r}_\text{V}$ could be determined experimentally by measuring the effective surface permittivity $\epsilon_\text{eff}(v_x)$[24,30,31] or the TM-wave surface impedance $Z_\text{p}(\omega, v_x)$[32,33] of the piezoelectric solid. They are found to be related by expressions (see Supplementary Note 3):

$$\bar{r}_\text{V} = i\frac{\epsilon_\text{eff} - \epsilon_0}{\epsilon_\text{eff} + \epsilon_0}, \quad \bar{r}_\text{V} = i\frac{1 + iv_x\epsilon_0 Z_\text{p}}{1 - iv_x\epsilon_0 Z_\text{p}}, \qquad (9)$$

where ϵ_0 is the vacuum permittivity. The effective surface permittivity concept is useful in the study of piezoelectric materials, for example for the generation and detection of acoustic waves by transducers[31] or for determining the gap wave modes between piezoelectric solids[24]. We find the symmetric and antisymmetric gap wave conditions can be simply expressed by $\bar{r}_\text{V} = \pm i\exp(k_x d)$, which are the poles of the transmission coefficient of Eq. (1) (Supplementary Note 3).

Numerical examples and physical interpretation of complete tunneling between identical ZnO crystals. We now turn to demonstrate the complete tunneling effect with numerical examples for two identical ZnO crystals, using the formalism developed before[23]. The first example is shown in Fig. 2, where the two crystals are separated with a scaled gap width of $kd = 0.01$, and are both rotated first with respect to the x-axis by $\vartheta = 46.89°$ and then to the z-axis by $\varphi = 88°$ (see Geng and Maasilta[23] for details on the crystal rotation procedure). The mode of the incident wave in this example is chosen to be the slowest quasi-transversal wave (ST), so that there exists a critical
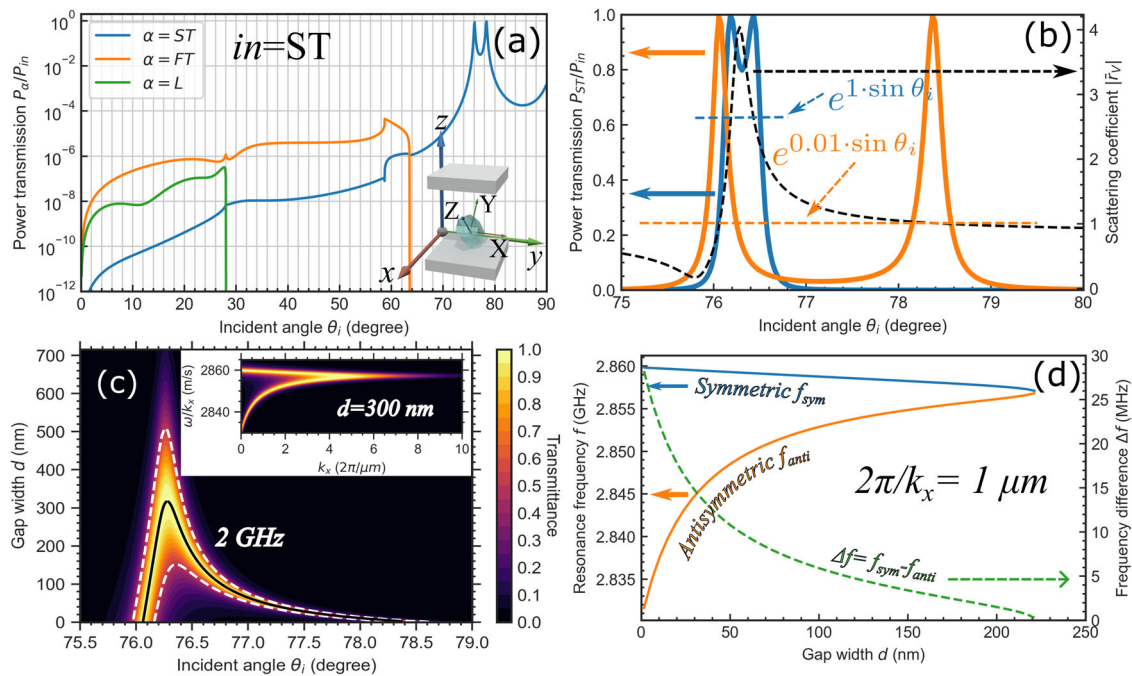
3

Fig. 2 Angular and gap width dependence of the power transmittance of an incoming ST wave. a Power transmittance P_α/P_{in} of the longitudinal $\alpha = $ L (green), the fast transverse $\alpha = $ FT (orange) and the slow transverse $\alpha = $ ST (blue) waves, for an incoming ST wave as function of the incident angle θ_i, for two identical ZnO crystals separated by a scaled gap $kd = 0.01$ and oriented with a zenith angle $\vartheta = 46.89°$ and an azimuth angle $\varphi = 88°$ (inset). We used the anisotropic crystal parameters $c_{11} = 20.97 \times 10^{10}$ Nm^{-2}, $c_{33} = 21.09 \times 10^{10}$ Nm^{-2}, $c_{44} = 4.247 \times 10^{10}$ Nm^{-2}, $c_{12} = 12.11 \times 10^{10}$ Nm^{-2}, $c_{13} = 10.51 \times 10^{10}$ Nm^{-2}, $c_{66} = (c_{11} - c_{12})/2$, $\epsilon_{xx} = 8.55\epsilon_0$, $\epsilon_{zz} = 10.2\epsilon_0$, $e_{x5} = -0.48$ Cm^{-2}, $e_{z1} = -0.573$ Cm^{-2}, $e_{z3} = 1.32$ Cm^{-2}, and the density $\rho = 5680$ kgm^{-3}, taken from Auld[19]. **b** Zoomed view on the peaks of the transmittance (left axis) with two values $kd = 1$ (blue solid line) and $kd = 0.01$ (orange solid line). The single surface reflection coefficient $|\bar{r}_V|$ curve (black dashed line) is overlayed (right axis) together with $\exp(k_x d) = \exp(\sin\theta_i)$ (blue horizontal dashed line) and $\exp(k_x d) = \exp(0.01\sin\theta_i)$ (orange horizontal dashed line) to demonstrate the resonance condition, Eq. (8), for the two scaled gaps, respectively. **c** Power transmittance (color scale) as a function of incident angle θ_i and gap width d at a fixed frequency of 2 GHz (main panel), and as a function of ω/k_x and k_x, with a fixed $d = 300$ nm (inset panel). The black solid line represents the resonance condition (Eq. (8)), and the white dashed lines indicate 50% power transmittance. **d** Frequencies of the symmetric (blue) and antisymmetric (orange) resonances as functions of gap width d for a fixed k_x of $2\pi/k_x = 1\,\mu$m, where the symmetry refers to the shape of the electrical potential function in the gap. The green dashed line shows the frequency difference between the two resonances.

incident angle beyond which only one bulk transmitted wave can be found, thus satisfying the general condition for complete tunneling.

In Fig. 2a, we plot the transmittance into each bulk mode P_α/P_{in} as a function of the incident angle θ_i, where α can be the quasi-longitudinal (L), the fast quasi-transversal (FT) or the slow quasi-transversal (ST) mode, categorized based on their phase velocities. We see that for most angles, transmittance is low, except for the two sharp transmission peaks for the ST mode giving exactly unity transmission at angles between 75° and 80°. Abrupt cut-offs are visible for the transmitted L and FT modes, corresponding to the critical incident angles $\theta_{L_c} \approx 28°$ and $\theta_{FT_c} \approx 63.5°$. Beyond these critical angles, the corresponding modes become evanescent, bound on the surface of the solid with no direct energy transmission into the bulk.

Figure 2b provides a zoomed view on the resonant transmission peaks, now with two different scaled gap values $kd = 1$ (blue solid line) and $kd = 0.01$ (orange solid line), with an overlay of the $|\bar{r}_V|$ curve (black dashed line), helping us also to understand the doublet structure. The two additional horizontal dashed lines represent the values of the RHS of Eq. (8) for the two kd values, whereas the dashed black curve represents the LHS of Eq. (8). It is clear that the unity transmission occurs where the resonance condition is valid, proving consistency between the analytical theory and the numerical approach. In addition, we see that with the increase of the scaled gap width from 0.01 to 1, the separation

of the peaks is reduced, and with a further increase the two solutions would merge into one at the maximum of $|\bar{r}_V|$. With this particular ZnO crystal orientation, this maximum is about 4 as shown in the plot, which leads to a maximum gap width of $kd \approx 1.4$ to observe complete tunneling (merged unity transmission peak). For ZnO (ST wave velocity $v = 2780$ m/s), and a 2 GHz frequency relevant for device applications, this corresponds to a quite long physical distance of $d = 300$ nm with the parameters and the orientation used in the example.

In addition, it is also useful to briefly discuss how sensitive the power transmittance is to deviations from the resonance condition, based on the above numerical example. For a fixed frequency of 2 GHz, the transmittance as a function of both the incident angle θ_i and the gap width d is presented in Fig. 2c. We see that when the vacuum gap is small, e.g., $d < 100$ nm, the two resonances are well separated and are sensitive to deviations of both d and θ_i. For example, a 50% drop in transmittance (white dashed lines) occurs within a 10 nm change in d or a 0.1 degree change in θ_i for the right branch. However, the merging of the two resonances leads to a higher deviation tolerance. $\theta_i = 76.4°$ is an example, where the transmittance remains higher than 50% for a wide range 150 nm $< d < 500$ nm, significantly relaxing the constraint for the gap width control in measuring the tunneling. Similar discussion can also be applied for a fixed gap width, for which the transmittance becomes a function of the angular frequency ω and the in-plane wave vector k_x, as illustrated in the inset of panel (c).
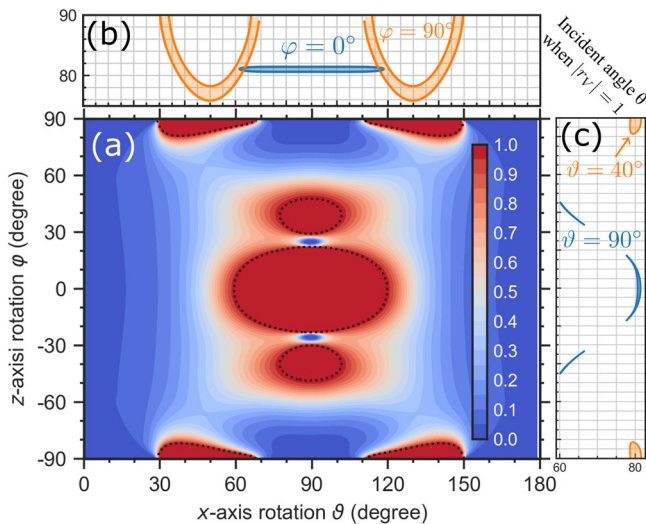
Fig. 3 Crystal rotation map for complete tunneling between ZnO crystals. **a** Color scale of the ST-to-ST mode maximum power transmittance P_{ST}/P_{in} over all incident angles, plotted as function of crystal rotation angles ϑ and φ for anisotropic ZnO. The dotted lines encircle the regions where $|\bar{r}_V| > 1$. **b**, **c** show the range of θ_i where $|\bar{r}_V| > 1$ for two fixed φ (**b**), or ϑ (**c**). Here, we fix $k_x d = kd \sin\theta_i$ instead of kd, as complete tunneling can be achieved by tuning k_x either by changing the incident angle θ_i or by the angular frequency ω.

Furthermore, it is possible to take advantage of the resonances in experiments and potential applications, such as the precise control of a gap distance. By exciting a bulk wave with a known in-plane wave vector k_x (for example with an interdigital transducer of finger spacing $2\pi/k_x$[31]), the frequencies of the two tunneling resonances become functions of the gap distance, as demonstrated for our numerical example case in Fig. 2d. We see that while the higher-frequency resonance f_{sym} depends weakly on d, the lower-frequency resonance f_{anti} is highly sensitive to d, with $\partial f/\partial d \approx 0.3$ MHz/nm at $d < 20$ nm. In addition, the frequency difference $\Delta f = f_{sym} - f_{anti}$ (green dashed line, right axis scale) is also sensitive to d, reaching a responsivity ~0.5 MHz/nm at $d < 20$ nm. Such relations can be envisioned to be used not only to experimentally demonstrate acoustic wave tunneling, but also to control a buried nanoscale gap distance with nanometer accuracy.

In general, the complete resonant tunneling can take place for a range of crystal orientations. In Fig. 3, we show the numerically calculated maximal power transmittance P_{ST}/P_{in} (over all θ_i) of an incident ST mode to a transmitted ST mode, as a function of all possible crystal rotations (ZnO has a crystallographic 6 mm system with uniaxial symmetry[19], hence all the unique orientations of the crystal can be represented by the direction of the crystal c-axis (Z-axis) using a zenith angle $\vartheta \in (0°, 180°)$ and an azimuth angle $\varphi \in (-90°, 90°)$), using again parameters for anisotropic ZnO[19] and a fixed scaled gap $k_x d = 0.01$. We find a significant parameter space for orientations, with multiple separate regions, where complete tunneling is possible (dark red regions). To validate the consistency of the numerics with the analytical condition, Eq. (8), we also plot a set of dotted contour lines in Fig. 3a to encircle the orientations satisfying $|\bar{r}_V| > 1$, where unity transmission is possible, finding excellent agreement. Another observation is that the incident angle θ_i satisfying complete tunneling varies for different crystal orientations (Fig. 3b, c), reaching as low values as 60° in some cases (Fig. 3c).

To understand the physics, we first consider the three ellipsoidal unity transmission areas around $\vartheta = 90°$ (Fig. 3). Inside these areas, the incident ST waves are not pure shear waves

and therefore couple to the other partial waves (L, FT) at the surface. As a result, when the incoming ST wave has an incident angle beyond the critical angle of the FT mode, the reflected FT wave becomes evanescent, with its energy concentrated on the surface. For those orientations the FT-mode waves are predominately polarized in the direction of the c-axis, the direction of the piezoelectric dipole, creating a strong piezoelectric response. That excites large electric potential differences on the surface and hence gives rise to a strong electric coupling across the gap, which finally enables the resonant transmission. On the other hand, when the azimuth rotations approach $\varphi = \pm 90°$ with $\vartheta = 90°$, the c-axis aligns with the x-axis and the ST mode becomes a pure shear mode, polarized perpendicular to the sagittal plane. Then the incident ST waves are very weakly piezoelectric, and also decouple from all other partial modes.

Other features can also be observed in Fig. 3a. Nodes having low transmission at around $\varphi = \pm 25°$ and $\vartheta = 90°$ appear. This is because the electric potential excited by the reflected FT wave mode change polarity around these nodes, leading to minimized potential differences and weak coupling between the two surfaces. In addition, unity transmission is also observed in four small areas around $\varphi = \pm 90°$, where the single surface reflection coefficient $\bar{r}^{(1)}_{ST \to FT}$ of the reflected FT partial waves increases significantly. This indicates an enhanced mode conversion between the ST and FT partial wave modes at these orientations, providing large electric potential differences on the solid-vacuum interface again via the evanescent FT wave, leading to strong tunneling signal. A more detailed discussion of the physical interpretation of the resonance can be found in Supplementary Note 4.

Our numerical formalism can also be applied to the particular case studied with a simplified model before[5], the details of which can be found in Supplementary Note 5. We do not find complete tunneling for the incoming modes and the crystal orientation in question, in contradiction to previous work[5].

Conclusions

In conclusion, we have analytically and numerically proven it is possible for acoustic waves to completely tunnel across a vacuum gap between two piezoelectric solids, up to gap sizes of about a wavelength. We showed that such complete tunneling, with unity power transmittance, is possible only if one transmitted partial bulk mode is excited, it being the same mode as the incident wave. We derived a simple resonance tunneling condition for the complete tunneling effect, Eq. (8), and proved its validity and range of applicability with numerical examples for arbitrarily rotated ZnO crystals. As this is a strong and not a rare effect, it could have an impact in future acoustic wave devices, as well as in other application areas concerning phonons, such as controlling heat transport, optomechanics and quantum information science.

Methods

Extended Stroh formalism and multiple reflection approach. In piezoelectric solids, the dynamics of a propagating plane (bulk) wave $\sim \exp(-i\mathbf{k} \cdot \mathbf{r} + i\omega t)$ are governed by the elastic equation of motion $\nabla \cdot \boldsymbol{\sigma} = \rho \partial^2 \mathbf{u}/\partial t^2$ and Gauss's law $\nabla \cdot \mathbf{D} = 0$, together with the piezoelectric constitutive relations[19]:

$$\begin{aligned}
\boldsymbol{\sigma} &= \mathbf{c}^E : \mathbf{S} - \mathbf{e} \cdot \mathbf{E} \\
\mathbf{D} &= \mathbf{e} : \mathbf{S} + \boldsymbol{\epsilon}^S \cdot \mathbf{E}
\end{aligned} \tag{10}$$

where $\mathbf{S}, \boldsymbol{\sigma}, \mathbf{u}, \mathbf{D}$ are the elastic strain, elastic stress, mechanical displacement and electric displacement fields, $\rho, \mathbf{c}^E, \mathbf{e}, \boldsymbol{\epsilon}^S$ are the mass density, elastic stiffness tensor at constant electric field, piezoelectric stress tensor and electric permittivity tensor at constant strain, respectively. The double dot product indicates summation over paired indices between second-rank and higher-rank tensors, and the strain-displacement relation reads as $S_{ij} = (\partial u_i/\partial r_j + \partial u_j/\partial r_i)/2$.

An incident plane wave is scattered into a linear combination of partial waves at an interface, which are either reflected or transmitted. The general solutions of such

5

partial waves that satisfy the governing equations take the expressions[34–36]:

$$\mathbf{u} = \sum_\alpha b_\alpha \mathbf{A}_\alpha e^{-i(k_x x + k_y y + p_\alpha k_x z - \omega t)}$$

$$\Phi = \sum_\alpha b_\alpha \phi_\alpha e^{-i(k_x x + k_y y + p_\alpha k_x z - \omega t)}$$

$$\mathbf{n} \cdot \boldsymbol{\sigma} = i k_x \sum_\alpha b_\alpha \mathbf{L}_\alpha e^{-i(k_x x + k_y y + p_\alpha k_x z - \omega t)} \quad (11)$$

$$\mathbf{n} \cdot \mathbf{D} = i k_x \sum_\alpha b_\alpha D_\alpha e^{-i(k_x x + k_y y + p_\alpha k_x z - \omega t)},$$

in which $\mathbf{n}$ is the unit vector of the z-axis. $\mathbf{A}_\alpha, \phi_\alpha, \mathbf{L}_\alpha, D_\alpha$ are the normalized constants describing the polarization vector, the electric potential, the traction force and the normal projection of the electric displacement of a partial wave mode α, respectively. b_α are dimensionless amplitudes of the partial waves, and $p \equiv k_z/k_x$. To avoid redundant writing in the following expressions, we omit the common phase factor $\exp(-ik_x x - ik_y y + i\omega t)$ shared by all solutions.

In this study, we solved these governing equations under the framework of extended Stroh formalism[23], in which Eq. (10) is combined and rearranged into an eight-dimensional eigenvalue problem[37,38] in the form of:

$$\mathbf{N}(v_x)\boldsymbol{\xi}_\alpha = p_\alpha \boldsymbol{\xi}_\alpha, \quad (12)$$

where $\mathbf{N}$ is 8×8 real matrix and $v_x \equiv \omega/k_x$ is the x-component of the phase velocity. Generally, eight linearly independent eigenvectors $\boldsymbol{\xi}_\alpha = [\mathbf{A}_\alpha, \phi_\alpha, \mathbf{L}_\alpha, D_\alpha]^T$ and corresponding eigenvalues p_α can be obtained for partial wave modes $\alpha = 1, ..., 8$. These eigenvectors follow the orthonormalization and completeness conditions:

$$\boldsymbol{\xi}_\alpha^T \hat{\mathbf{T}} \boldsymbol{\xi}_\beta = \delta_{\alpha\beta} \quad (13)$$

$$\sum \boldsymbol{\xi}_\alpha \otimes \hat{\mathbf{T}} \boldsymbol{\xi}_\alpha = \hat{\mathbf{I}}_{8\times8}, \quad (14)$$

where the operator $\otimes$ denotes the outer product of two matrices, $\delta_{\alpha\beta}$ is the Kronecker delta, $\hat{\mathbf{I}}_{8\times8}$ is 8×8 unit matrix, and $\hat{\mathbf{T}}$ takes the form:

$$\hat{\mathbf{T}} = \begin{bmatrix} \mathbf{O}_{4\times4} & \hat{\mathbf{I}}_{4\times4} \\ \hat{\mathbf{I}}_{4\times4} & \mathbf{O}_{4\times4} \end{bmatrix} \quad (15)$$

where $\mathbf{O}_{4\times4}$ and $\hat{\mathbf{I}}_{4\times4}$ are 4×4 zero and unity matrices.

The continuity of the electric potential ($\Phi^{(i)} = \Phi_V$, where the subscript $i = 1, 2$ indicates the medium index and the subscript V indicates the vacuum) and the normal component of electric displacement ($\mathbf{n} \cdot \mathbf{D}^{(i)} = \mathbf{n} \cdot \mathbf{D}_V$), as well as the condition of a mechanically free surface ($\mathbf{n} \cdot \boldsymbol{\sigma}^{(i)} = \mathbf{0}$) enforce the boundary conditions of the two solid-vacuum interfaces:

$$b_{in}^{(1)} \mathbf{U}_{in}^{(1)} + \sum_{\alpha=1}^{4} b_\alpha^{(1)} \mathbf{U}_\alpha^{(1)} = b_{V_+} \mathbf{U}_{V_+} + b_{V_-} \mathbf{U}_{V_-},$$

$$\sum_{\alpha=1}^{4} \tilde{b}_\alpha^{(2)} \mathbf{U}_\alpha^{(2)} = b_{V_+} \mathbf{U}_{V_+} e^{-k_x d} + b_{V_-} \mathbf{U}_{V_-} e^{k_x d}, \quad (16)$$

in which we introduce 5×1 column vectors $\mathbf{U}_\gamma^{(i)} = [\phi_\gamma^{(i)}, D_\gamma^{(i)}, \mathbf{L}_\gamma^{(i)}]^T$ for wave modes $\gamma = $ in, α, where the subscript in indicates the incident wave mode, $\alpha = 1, ..., 4$ corresponds to four physically allowed wave modes in their corresponding medium $i = 1, 2, \mathbf{U}_{V_\pm} = [\phi_{V_\pm}, D_{V_\pm}, 0, 0, 0]^T$, and $\tilde{b}_\alpha^{(2)} \equiv b_\alpha^{(2)} \exp(ip_\alpha^{(2)} k_x d)$ for simplicity. In the vacuum region, the electric potential and displacement fields take the form:

$$\Phi_V(z) = b_{V_+} \phi_{V_+} e^{k_x z} + b_{V_-} \phi_{V_-} e^{-k_x z}$$

$$\mathbf{n} \cdot \mathbf{D}_V(z) = -\epsilon_0 k_x b_{V_+} \phi_{V_+} e^{k_x z} + \epsilon_0 k_x b_{V_-} \phi_{V_-} e^{-k_x z}, \quad (17)$$

where $\phi_{V_\pm} = 1/\sqrt{\pm 2i\epsilon_0}$, noting the normalization condition for the vacuum mode $2\phi_{V_\pm} D_{V_\pm} = 1$.

The amplitude factors $b_\alpha^{(i)}$ can be solved from the boundary conditions of Eq. (16), following the multiple reflection method introduced in Geng and Maasilta[23]: the single surface reflection ($\bar{r}_{in\to\alpha}^{(i)}, \bar{r}_V^{(i)}$) and transmission ($\bar{t}_{V\to\alpha}^{(i)}, \bar{t}_{in\to V}^{(i)}$) coefficients are calculated first via scattering matrices $\mathbb{S}^{(i)}$ for solid $i = 1, 2$, and the total transmission coefficient t_α for a partial mode α is then obtained by coupling the single surface coefficients with a multiple reflection factor $f_m(d)$, which explicitly depends on the gap distance d. We note here that the overlined single surface coefficients describe the scattering of the electroacoustic wave as if there is no second adjacent solid.

The 5×2 scattering matrices $\mathbb{S}^{(1)}$ and $\mathbb{S}^{(2)}$ take the following form:

$$\mathbb{S}^{(1)} = \begin{bmatrix} \bar{\mathbf{r}}^{(1)} & \bar{\mathbf{t}}^{(1)} \\ \bar{t}_{in\to V}^{(1)} & \bar{r}_V^{(1)} \end{bmatrix}$$

$$= [\mathbf{U}_1^{(1)}, ..., \mathbf{U}_4^{(1)}, -\mathbf{U}_{V_+}]^{-1} [-\mathbf{U}_{in}^{(1)}, \mathbf{U}_{V_-}],$$

$$\mathbb{S}^{(2)} = \begin{bmatrix} \bar{\mathbf{r}}^{(2)} & \bar{\mathbf{t}}^{(2)} \\ \bar{t}_{in\to V}^{(2)} & \bar{r}_V^{(2)} \end{bmatrix}$$

$$= [\mathbf{U}_1^{(2)}, ..., \mathbf{U}_4^{(2)}, -\mathbf{U}_{V_-}]^{-1} [\mathbf{U}_{in}^{(2)}, \mathbf{U}_{V_+}] \quad (18)$$

where the expression $\bar{\mathbf{r}}^{(i)} = [\bar{r}_{in\to1}^{(i)}, ..., \bar{r}_{in\to4}^{(i)}]^T$ and $\bar{\mathbf{t}}^{(i)} = [\bar{t}_{V\to1}^{(i)}, ..., \bar{t}_{V\to4}^{(i)}]^T$ are the single surface reflection and transmission coefficients of modes $\alpha = 1, ..., 4$.

The total transmission coefficient t_α from an incoming bulk wave in solid 1 into a partial wave of mode α in solid 2 can be obtained as:

$$t_\alpha \equiv \frac{\tilde{b}_\alpha^{(2)}}{b_{in}^{(1)}} = \bar{t}_{in\to V}^{(1)} \bar{t}_{V\to\alpha}^{(2)} f_m(d) \quad (19)$$

where the multiple reflection factor is $f_m(d) = [\exp(k_x d) - \bar{r}_V^{(1)} \bar{r}_V^{(2)} \exp(-k_x d)]^{-1}$. Equation (19) is identical to Eq. (1) in the main text.

The time-averaged transmitted power flow density in the direction normal to the surfaces from solid 1 to 2 can be expressed by the real part of the piezoelectric Poynting vector in the normal direction[34]:

$$P_\alpha = -\frac{\omega k_x}{4} |b_\alpha|^2 \boldsymbol{\xi}_\alpha^T \hat{\mathbf{T}} \boldsymbol{\xi}_\alpha^*. \quad (20)$$

For transmitted homogeneous (bulk) waves, $\boldsymbol{\xi}_\alpha^T \hat{\mathbf{T}} \boldsymbol{\xi}_\alpha^* = \pm \boldsymbol{\xi}_\alpha^T \hat{\mathbf{T}} \boldsymbol{\xi}_\alpha = \pm 1$, due to the Stroh-normalization condition (Eq. (13)). Therefore $|t_\alpha|^2$ can be interpreted as the power flow ratio (the transmittance) of the transmitted bulk partial wave over the incident wave in the normal direction:

$$P_\alpha = |t_\alpha|^2 P_{in}. \quad (21)$$

Data availability

All relevant data are available from the authors upon request.

Code availability

All relevant code for simulations are available from the authors upon request.

References

1. Kim, K. et al. Radiative heat transfer in the extreme near field. *Nature* **528**, 387 (2015).
2. Kloppstech, K. et al. Giant heat transfer in the crossover regime between conduction and radiation. *Nat. Commun.* **8**, 14475 (2017).
3. Cui, J. et al. Nanofabrication with the thermal AFM metallic tip irradiated by continuous laser. *Integr. Ferroelectr.* **179**, 140 (2017).
4. Jarzembski, A. et al. Role of acoustic phonon transport in near- to asperity-contact heat transfer. *Phys. Rev. B* **106**, 205418 (2022).
5. Prunnila, M. & Meltaus, J. Acoustic phonon tunneling and heat transport due to evanescent electric fields. *Phys. Rev. Lett.* **105**, 125501 (2010).
6. Sellan, D. P. et al. Phonon transport across a vacuum gap. *Phys. Rev. B* **85**, 024118 (2012).
7. Persson, B. N., Volokitin, A. I. & Ueba, H. Phononic heat transfer across an interface: thermal boundary resistance. *J. Phys.: Condens. Matter* **23**, 045009 (2011).
8. Chiloyan, V., Garg, J., Esfarjani, K. & Chen, G. Transition from near-field thermal radiation to phonon heat conduction at sub-nanometre gaps. *Nat. Commun.* **6**, 6755 (2015).
9. Budaev, B. V. & Bogy, D. B. On the role of acoustic waves (phonons) in equilibrium heat exchange across a vacuum gap. *Appl. Phys. Lett.* **99**, 053109 (2011).
10. Xiong, S. et al. Classical to quantum transition of heat transfer between two silica clusters. *Phys. Rev. Lett.* **112**, 114301 (2014).
11. Ezzahri, Y. & Joulain, K. Vacuum-induced phonon transfer between two solid dielectric materials: illustrating the case of Casimir force coupling. *Phys. Rev. B* **90**, 115433 (2014).
12. Sasihithlu, K., Pendry, J. B. & Craster, R. V. Van der Waals force assisted heat transfer. *Z. Naturforsch. A* **72**, 181 (2017).
13. Pendry, J. B., Sasihithlu, K. & Craster, R. V. Phonon-assisted heat transfer between vacuum-separated surfaces. *Phys. Rev. B* **94**, 075414 (2016).
14. Volokitin, A. I. Effect of an electric field in the heat transfer between metals in the extreme near field. *JETP Lett.* **109**, 749 (2019).
15. Volokitin, A. I. Contribution of the acoustic waves to near-field heat transfer. *J. Phys.: Condens. Matter* **32**, 215001 (2020).
16. Biehs, S. A., Kittel, A. & Ben-Abdallah, P. Fundamental limitations of the mode temperature concept in strongly coupled systems. *Z. Naturforsch. A* **75**, 803 (2020).

17. Alkurdi, A. et al. Thermal transport across nanometre gaps: phonon transmission vs. air conduction. *Int. J. Heat. Mass Transf.* **158**, 119963 (2020).

18. Tokunaga, T. et al. First-principles calculations of phonon transport across a vacuum gap. *Phys. Rev. B* **105**, 045410 (2022).

19. Auld, B. *Acoustic Fields and Waves in Solids* 2nd edn (Krieger, 1990).

20. Kaliski, S. The passage of an ultrasonic wave across a contactless junction between two piezoelectric bodies. *Proc. Vibr. Probl. Warsaw* **7**, 95 (1966).

21. Balakirev, M. & Gorchakov, A. Leakage of an elastic wave across a gap between piezoelectrics. *Fiz. Tverd. Tela* **19**, 571 (1977) [*Sov. Phys. Solid State* **19**, 327 (1977)].

22. Balakirev, M., Bogdanov, S. & Gorchakov, A. Tunneling of ultrasonic wave through a gap between lithium iodate crystals. *Fiz. Tverd. Tela* **20**, 587 (1978) [*Sov. Phys. SolidState* **20**, 338 (1978)].

23. Geng, Z. & Maasilta, I. J. Acoustic wave tunneling across vacuum gap between two piezoelectric crystals with arbitrary symmetry and orientation. *Phys. Rev. Res.* **4**, 033073 (2022).

24. Darinskii, A. N. & Weihnacht, M. Gap acousto-electric waves in structures of arbitrary anisotropy. *IEEE Trans. Ultrason. Ferroelectr. Freq. Control* **53**, 412 (2006).

25. Born, M., Wolf, E. & Bhatia, A. B. *Principles of Optics: Electromagnetic Theory of Propagation, Interference, and Diffraction of Light* 7th edn (Cambridge University Press, 2019).

26. Every, A. G. & Neiman, V. I. Reflection of the electroacoustic waves in piezoelectric solids: mode conversion into four bulk waves. *J. Appl. Phys.* **71**, 6018 (1992).

27. Joulain, K., Mulet, J.-P., Marquier, F., Carminati, R. & Greffet, J.-J. Surface electromagnetic waves thermally excited: radiative heat transfer, coherence properties and Casimir forces revisited in the near field. *Surf. Sci. Rep.* **57**, 59 (2005).

28. Pendry, J. B. Radiative exchange of heat between nanostructures. *J. Phys.: Condens. Matter* **11**, 6621 (1999).

29. Biehs, S.-A., Rousseau, E. & Greffet, J.-J. Mesoscopic description of radiative heat transfer at the nanoscale. *Phys. Rev. Lett.* **105**, 234301 (2010).

30. Maugin, G. *Continuum Mechanics of Electromagnetic Solids* (Elsevier, 1988).

31. Milsom, R. F., Reilly, N. H. & Redwood, M. Analysis of generation and detection of surface and bulk acoustic waves by interdigital transducers. *IEEE Trans. Sonics Ultrason.* **SU-24**, 147 (1977).

32. Ingebrigtsen, K. A. Surface waves in piezoelectrics. *J. Appl. Phys.* **40**, 2681 (1969).

33. Zhang, Y., Desbois, J. & Boyer, L. New method to characterize the surface-generated bulk acoustic waves in piezoelectric substrates. *J. Acoust. Soc. Am.* **92**, 2499 (1992).

34. Al'shits, V. I., Darinskii, A. N. & Shuvalov, A. L. Theory of reflection of acoustoelectric waves in a semiinfinite piezoelectric medium. I. Metallized surface. *Kristallografiya* **34**, 1340 (1989) [*Sov. Phys. Crystallogr.* **34**, 808 (1989)].

35. Al'shits, V. I., Darinskii, A. N. & Shuvalov, A. L. Theory of reflection of acoustoelectric waves in a semiinfinite piezoelectric medium. II. Nonmetallized surface. *Kristallografiya* **35**, 7 (1990) [*Sov. Phys. Crystallogr.* **35**, 1 (1990)].

36. Al'shits, V. I., Darinskii, A. N. & Shuvalov, A. L. Theory of reflection of acoustoelectric waves in a semiinfinite piezoelectric medium. III. Resonance reflection in the neighborhood of a branch of outflowing waves. *Kristallografiya* **36**, 284 (1991) [*Sov. Phys.Crystallogr.* **36**, 145 (1991)].

37. Barnett, D. M. & Lothe, J. Dislocations and line charges in anisotropic piezoelectric insulators. *Phys. Status Solidi B* **67**, 105 (1975).

38. Lothe, J. & Barnett, D. M. Integral formalism for surface waves in piezoelectric crystals. Existence considerations. *J. Appl. Phys.* **47**, 1799 (1976).

Acknowledgements

Author contributions

Z.G. and I.J.M. conceived the idea, carried out the analytical derivations and wrote the manuscript. Z.G. carried out all the numerical calculations.

Competing interests

The authors declare no competing interests.

Additional information

Supplementary information The online version contains supplementary material available at https://doi.org/10.1038/s42005-023-01293-y.

Correspondence and requests for materials should be addressed to Zhuoran Geng or Ilari J. Maasilta.

Peer review information *Communications Physics* thanks Takuma Shiga, Svend Age Biehs and the other, anonymous, reviewer(s) for their contribution to the peer review of this work. A peer review file is available.

Reprints and permission information is available at http://www.nature.com/reprints

Publisher's note Springer Nature remains neutral with regard to jurisdictional claims in published maps and institutional affiliations.